Numerical Investigation of Photon-Pair Generation in Periodically Poled $MTiOXO_4$ (M = K, Rb, Cs; X = P, As)

Fabian Laudenbach,[1,2,*] Rui-Bo Jin,[3] Chiara Greganti,[2] Michael Hentschel,[1] Philip Walther,[2] and Hannes Hübel[1]

[1]*Security & Communication Technologies, Center for Digital Safety & Security, AIT Austrian Institute of Technology GmbH, Donau-City-Strasse 1, 1220 Vienna, Austria*

[2]*Quantum Optics, Quantum Nanophysics and Quantum Information, Faculty of Physics, University of Vienna, Boltzmanngasse 5, 1090 Vienna, Austria*

[3]*Laboratory of Optical Information Technology, Wuhan Institute of Technology, Wuhan 430205, China*

(Received 14 June 2017; revised manuscript received 4 August 2017; published 31 August 2017)

We present a detailed numerical investigation of five nonlinear materials and their properties regarding photon-pair creation using parametric down-conversion. Periodic poling of ferroelectric nonlinear materials is a convenient way to generate collinearly propagating photon pairs. Most applications and experiments use the well-known potassium titanyl phosphate ($KTiOPO_4$, PPKTP) and lithium niobate ($LiNbO_3$, PPLN) crystals for this purpose. We provide a profound discussion on the family of KTP-isomorphic nonlinear materials, including KTP itself but also the much less common $CsTiOAsO_4$, $KTiOAsO_4$, $RbTiOAsO_4$, and $RbTiOPO_4$. We discuss the way in which these crystals can be used for the creation of spectrally pure down-conversion states and the generation of crystal-intrinsic polarization and frequency entanglement. The investigation of the new materials discloses an entirely different range of promising experimental setups, in some cases even outperforming the established materials PPLN and PPKTP.

DOI: 10.1103/PhysRevApplied.8.024035

I. INTRODUCTION

Photon-pair generation by spontaneous parametric down-conversion (SPDC), a nonlinear process where a high-energy photon (mostly referred to as *pump*) decays into two low-energy photons (*signal* and *idler*), is a convenient approach for realizing heralded single-photon sources or quantum entanglement, vital for photonic quantum-information applications. In particular, SPDC in periodically poled nonlinear media allows for collinear propagation and, therefore, high collection efficiencies. This technique is often referred to as quasi phase matching (QPM). Popular nonlinear crystals suited for periodic poling are *potassium titanyl phosphate* ($KTiOPO_4$, PPKTP), *lithium niobate* ($LiNbO_3$, PPLN), and *lithium tantalate* ($LiTaO_3$, PPLT).

Most applications of photon-pair generation require a high spectral quantum purity which is equivalent to *frequency-uncorrelated* photon pairs. However, in general, SPDC states do contain frequency entanglement, which, when one of the substates is traced out (i.e., by detection of one photon), puts the other one into a mixed state. In order to remove these correlations in the joint spectral distribution, many experiments use narrow bandpass filters [1] or single-mode fibers [2], which transmit only the uncorrelated parts of the spectrum. Unfortunately, bandpass filtering obviously comes with a drastic decrease in count rates and heralding efficiency since a large quantity of generated photons is discarded. As an alternative approach, the SPDC process can be carefully designed such that the generated SPDC state is *a priori* frequency uncorrelated; hence, no filtering is required in order to obtain high purity [3–15]. This method, however, is only feasible in a closed set of special cases, i.e., specific crystals allow for intrinsically pure SPDC states only at particular wavelength and polarization configurations. In addition, recently, three proposals were suggested [16–18] and implemented [19] in which the joint spectral distribution is shaped by a particular custom fabrication of the poled crystals. Owing to the early stage of development, it is difficult to evaluate the challenges in the fabrication process of identical crystals and, therefore, in the generation of independent identical photons.

As another highly interesting application of periodically poled crystals, we very recently demonstrated a way to generate photonic entanglement which is both very simplistic and efficient [20]. Up to now, efficient generation of collinear entangled photon pairs has required either two periodically poled crystals [21–25] or, alternatively, one single crystal pumped from two directions simultaneously [26–30]. Our alternative approach uses only one unidirectionally pumped PPKTP crystal, which drastically simplifies the experimental setup without any compromise in count rates or entanglement visibility. While a comparable concept has been proposed and demonstrated for modal phase matching on nonbirefringent Bragg-reflection waveguides [31,32], our method benefits from the relatively easy and widespread fabrication of quasi-phase-matching structures (which are cost efficient and insusceptible to

*fabian.laudenbach@ait.ac.at

fabrication errors) and the accurate spatial and spectral overlap of multiple decay channels (high brightness and entanglement visibility). It is based on the observation that a periodically poled crystal with a given grating constant, pumped with a given wavelength, can allow for two SPDC processes simultaneously, each exploiting its own quasi-phase-matching order—an effect we refer to as *collinear double down-conversion* (CDDC). Unfortunately, this method allows for only a limited set of possible wavelength configurations, depending on the material properties of the respective nonlinear crystal. This means that, although there is a large set of possible realizations, the generated wavelengths cannot be chosen completely arbitrarily. However, the more nonlinear materials there are available, the greater the repertory of possible configurations.

In the past, we performed extensive numerical investigations of well-known optical materials to find out to what extent they support the abovementioned techniques of frequency-uncorrelated SPDC states [3] and intrinsic entanglement [20]. We found a large set of *a priori* pure down-conversion processes in PPKTP, PPLN, and PPLT, encompassing all polarization configurations and various wavelength regimes. As for intrinsic entanglement by CDDC, we showed that PPKTP allows for numerous entangled-photon wavelengths in the near and midinfrared, as well as in the telecom regime.

Recently, we have started to extend the search for intrinsically pure SPDC states to other nonlinear materials, namely, CTA ($CsTiOAsO_4$), KTA ($KTiOAsO_4$), RTA ($RbTiOAsO_4$), and RTP ($RbTiOPO_4$) [33]. Being isomorphic to KTP, these crystals all share similar properties [34]. Like KTP, they belong to the *mm2* point group [35], and they have a similar transparency range and nonlinear tensor. Moreover, being ferroelectric materials, they allow for periodic poling just as KTP does. In our recent article, we presented the results of our numerical investigations of these materials, focusing on the important special case of frequency-degenerate and spectrally indistinguishable type-II down-conversion with high spectral purity. For this work, using our software QPMoptics [36], we investigate the properties of the KTP isomorphs more thoroughly, searching for inherently pure states in all possible polarization and wavelength configurations, including the nondegenerate ones. Moreover, we study their suitability for the abovementioned approach for intrinsic-entanglement generation. In conjunction with Ref. [3] (PPLN, PPLT, PPKTP), this article provides a comprehensive reference of a total of seven different optical media and in which way they can be used to generate pure photon states and/or intrinsic entanglement.

II. EFFECTIVE NONLINEAR COEFFICIENT

Table I lists the approximate effective nonlinear coefficients for all kinds of polarization configurations in five periodically poled nonlinear materials. The table illustrates the similarity of the five materials in terms of effective nonlinearity—and hence down-conversion efficiency.

III. CONFIGURATIONS OF HIGH INTRINSIC PURITY

The Hong-Ou-Mandel (HOM) visibility [39] of two photon states, represented as ρ_A and ρ_B, is upper-bounded by the relation [4]

$$V_{\mathrm{HOM}} \leq \mathrm{Tr}(\rho_A \rho_B) = \frac{P_A + P_B}{2} - \frac{\|\rho_A - \rho_B\|^2}{2} =: \frac{P_A + P_B}{2} - \Delta, \tag{1}$$

highlighting the role of quantum *purity* $P \in [0,1]$ and *distinguishability* $\Delta \in [0,1]$. [The matrix norm in Eq. (1) indicates the Frobenius norm: $\|\rho\| = \sqrt{\mathrm{Tr}(\rho^\dagger \rho)}$.] When the interfering photons originate from two identical sources, the purities coincide ($P_A = P_B =: P$) and the visibility simplifies to

$$V_{\mathrm{HOM}} \leq P - \Delta, \tag{2}$$

where $\Delta \geq 0$ when the signal of one pair interferes with the idler of another and $\Delta = 0$ when the corresponding photons

TABLE I. Effective nonlinearity coefficients of five kinds of periodically poled crystals in all polarization configurations, retrieved from the nonlinear optics code SNLO v.67 [37]. The superscripts of the nonlinear coefficients indicate the respective component of the nonlinear tensor d [38]. In all cases, a collinear propagation along the crystal's x axis is assumed. The letter o denotes polarization along the *ordinary* (the y) axis, while e denotes polarization along the *extraordinary* (the z) axis. Note that all numerical values in the table are to be understood as approximations since they vary slightly with the involved wavelengths and the material's doping.

SPDC type		Effective nonlinear coefficient $\lvert d_{\mathrm{eff}}\rvert$(pm V^{-1})				
		PPKTP	PPCTA	PPKTA	PPRTA	PPRTP
0	$o \to o + o$	0	0	0	0	0
	$e \to e + e$	$d^{33} \sim 9.5$	$d^{33} \sim 11.2$	$d^{33} \sim 9.6$	$d^{33} \sim 9.8$	$d^{33} \sim 9.6$
I	$o \to e + e$	0	0	0	0	0
	$e \to o + o$	$d^{24} \sim 2.4$	$d^{24} \sim 2.1$	$d^{24} \sim 2.3$	$d^{24} \sim 2.4$	$d^{24} \sim 2.4$
II	$o \to o + e$	$d^{32} \sim 2.4$	$d^{32} \sim 2.1$	$d^{32} \sim 2.3$	$d^{32} \sim 2.4$	$d^{32} \sim 2.4$
	$e \to o + e$	0	0	0	0	0

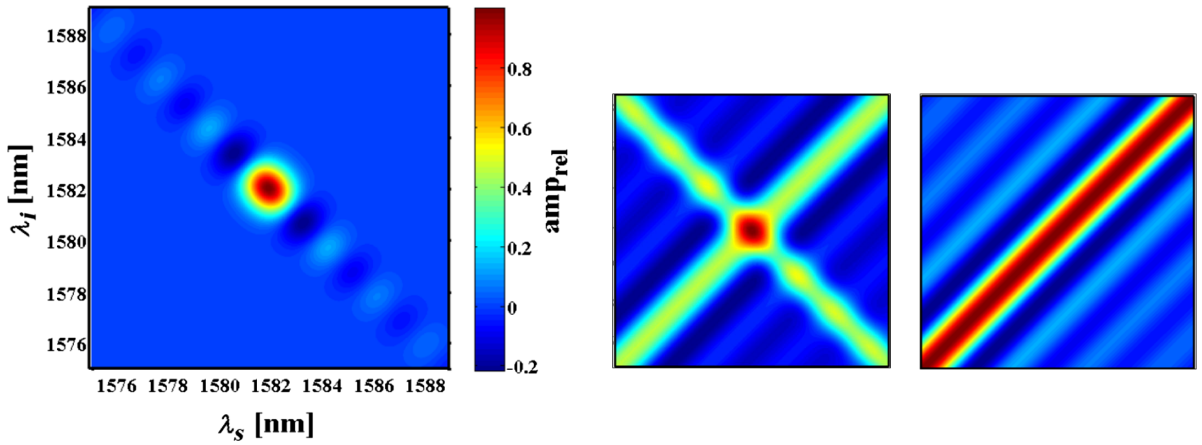

(a) JSA$=\mu\psi$; $D\approx 1$, $P=V_{\mathrm{HOM}}\sim 0.83$ (b) $\mu+\psi$ (c) ψ

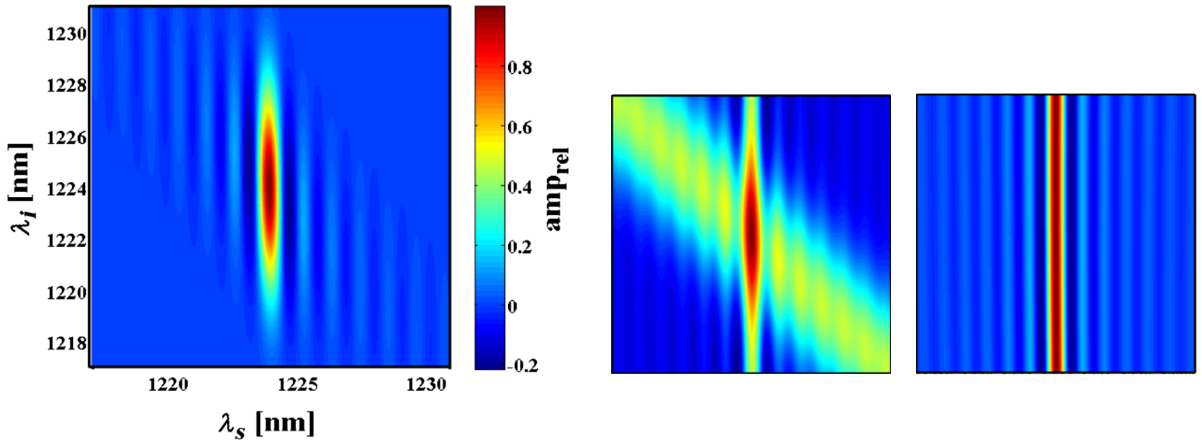

(d) JSA$=\mu\psi$; $D\approx 0$, $P\sim 0.96$, $V_{\mathrm{HOM}}\sim 0.11$ (e) $\mu+\psi$ (f) ψ

FIG. 1. Group-velocity matching in two examples. (a) represents the down-conversion 791 nm$(o)\rightarrow$ 1582 nm$(o)+$ 1582 nm(e) with the dispersion parameter $D\approx 1$. (d) corresponds to 612 nm$(o)\rightarrow$ 1224 nm$(o)+$ 1224 nm(e), with $D\approx 0$ (both in PPKTP). The signal and idler in (a) are spectrally fully indistinguishable, which is possible because of the orthogonal intersection of the pump and QPM amplitude (b). This constellation, however, requires the QPM amplitude ψ to be aligned diagonally in the wavelength plane (c), with the sidelobes of the sinc function being maximally spectrally correlated. This limits the maximal purity for spectrally indistinguishable SPDC states to $P=V_{\mathrm{HOM}}\sim 0.83$. On the other hand, when the QPM amplitude μ is aligned more vertically (f), the sidelobes are less spectrally correlated, which allows for a higher purity of $P>0.96$, but at the price of undermined indistinguishability and, therefore, signal-idler-interference visibility $V_{\mathrm{HOM}}\sim 0.1$. [The plots of $\mu+\psi$ (b),(d) serve the purpose only of illustrating the composition of the JSA and do not correspond to an actual physical quantity; the illustrations of the QPM amplitude ψ (c),(f) correspond to the same color mapping as the ones of the JSA (a),(c).]

of two pairs interfere (say, the two signal photons when the idler is used for heralding). Therefore, for identical heralded-photon sources, the distinguishability does not play a role and the visibility depends on the purity only.

The purity of a quantum state ρ is given by the trace of its square: $P=\mathrm{Tr}(\rho^2)$. For a pure bipartite system $|\Psi\rangle_{AB}$, expressed in terms of a Schmidt decomposition

$$|\Psi\rangle=\sum_i \sqrt{\lambda_i}\,|i_A\rangle|i_B\rangle, \tag{3}$$

the purity of the substates is equivalent to the sum of the squared Schmidt coefficients:

$$P_A=P_B=\sum_i \lambda_i^2 =: \frac{1}{K}, \tag{4}$$

where $K\geq 1$ is referred to the *Schmidt number*, a convenient measure for the entanglement in a bipartite system. The above equation illustrates nicely the relation between purity and entanglement. In a highly entangled state, there will be many nonzero coefficients λ in the Schmidt decomposition, yielding a high degree of entanglement K and, therefore, a low purity P. Conversely, in a factorable state, there is only one nonvanishing coefficient $\lambda=1$, yielding minimal entanglement $K=1$ and maximal purity $P=1$. Thus, a high spectral purity (as required for high interference

visibilities) is equivalent to low spectral correlations of the interfering substates.

The Schmidt coefficients of a down-conversion state $|\Psi\rangle$ can be obtained numerically by a singular-value decomposition (SVD) [4] of the joint spectral amplitude (JSA), which is the product of the pump amplitude μ and the quasi-phase-matching (QPM) amplitude ψ:

$$\mathrm{JSA} = \mu(\omega_s + \omega_i)\psi(\omega_s, \omega_i). \tag{5}$$

The QPM amplitude reads

$$\psi = e^{i\Delta k_m L/2}\,\mathrm{sinc}\left(\frac{\Delta k_m L}{2}\right). \tag{6}$$

Here, L is the length of the nonlinear crystal and Δk_m is the wave-vector difference

$$\begin{aligned}\Delta k_m &= k_p - k_s - k_i - \frac{2\pi m}{\Lambda} \\ &= \frac{\omega_s}{c}(n_p - n_s) + \frac{\omega_i}{c}(n_p - n_i) - \frac{2\pi m}{\Lambda},\end{aligned} \tag{7}$$

where n represents the refractive index, Λ is the poling period of the crystal, m is an odd integer referred to as QPM order, and we use the energy conservation $\omega_p = \omega_s + \omega_i$. Quasi phase matching is achieved when the sinc function in Eq. (6) equals 1—hence, when $\Delta k_m = 0$. Experimentally, we are not able to observe amplitudes directly. We therefore introduce the Schmidt number of the joint spectral *intensity* (JSI) K_{JSI}, obtained by a SVD of

$$\mathrm{JSI} = |\mathrm{JSA}|^2. \tag{8}$$

The QPM condition $\Delta k_m = 0$ needs to be met in order to generate a measurable output radiation with the desired wavelengths. On top of that, in order to allow for the generation of spectrally uncorrelated photon pairs, a SPDC setup needs to fulfil the *group-velocity-matching* (GVM) condition. GVM can be achieved in two different ways: The first manner is to match the group velocity of the pump photons with the group velocity of either the signal or the idler photons. In the second way, the group velocity of the pump photons coincides with the average group velocity of the signal and idler photons. The quality of GVM can be quantified by the dispersion parameter D [40]:

$$D = -\frac{\mathrm{GD}_p - \mathrm{GD}_s}{\mathrm{GD}_p - \mathrm{GD}_i} \quad \text{or} \tag{9a}$$

$$D = -\frac{\mathrm{GD}_p - \mathrm{GD}_i}{\mathrm{GD}_p - \mathrm{GD}_s}, \tag{9b}$$

depending on whether the pump velocity is matched to the signal velocity (the top line) or the idler velocity (the bottom line). GD represents the respective group delay, and hence the inverse group velocity in the optic medium. The two different types of GVM yield

$$D = 0, \quad \text{if } \mathrm{GD}_p = \mathrm{GD}_s \quad \text{or} \quad \mathrm{GD}_p = \mathrm{GD}_i, \tag{10a}$$

$$D = 1, \quad \text{if } \mathrm{GD}_p = (\mathrm{GD}_s + \mathrm{GD}_i)/2. \tag{10b}$$

A dispersion parameter of $D = 1$ corresponds to the QPM envelope amplitude ψ being diagonally aligned in the $\lambda_s - \lambda_i$ plane. This allows for a circular-shaped JSA, as required by multiphoton experiments where signal and idler are supposed to be spectrally pure *and* indistinguishable. Note, however, that maximal spectral indistinguishability of signal and idler to a certain degree compromises the state's purity, and vice versa. This drawback is due to the sidelobes of the sinc function in the QPM amplitude ψ, which are maximally correlated due the diagonal orientation of ψ. This impairment limits the intrinsic purity achievable with $D = 1$ to $P \sim 0.83$. On the other hand, when the GVM condition $D = 0$ is met, ψ is aligned horizontally or vertically in the wavelength plane, therefore carrying no spectral correlations. This gives rise to an

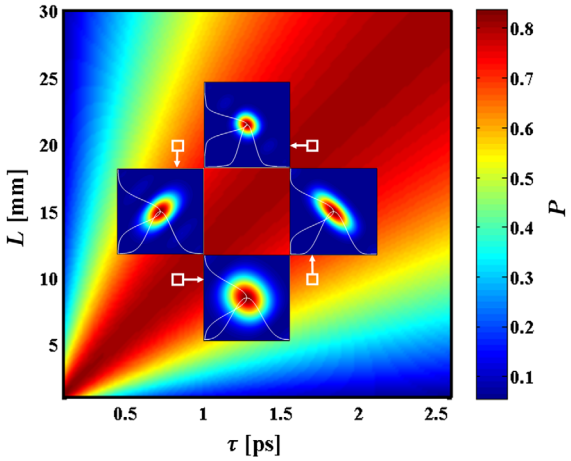

FIG. 2. Purity vs Gaussian-pulse duration τ and crystal length L. The example corresponds to the down-conversion 791 nm$(o) \rightarrow$ 1582 nm(o) + 1582 nm(e) in PPKTP. (Insets) The joint spectral intensity distribution corresponding to particular pairs of τ and L. The white curves in the insets illustrate the spectral intensity distribution of the signal (the horizontal axis) and the idler (the vertical axis). Although signal and idler are spectrally indistinguishable for any pair of τ and L's, a high intrinsic purity (i.e., frequency-uncorrelated daughter photons) can be obtained only by a mutual matching of the two. A short-pulsed (and therefore broadband) laser pumping a long crystal will generate frequency-correlated spectra (the left inset); a long-pulsed (hence, narrow band) laser in a short crystal will produce an anticorrelated signal and idler (the right inset). The top and bottom insets represent spectrally uncorrelated SPDC states, achieved by an appropriate matching of pulse duration and crystal length. (A similar figure was previously published in Ref. [3] and was modified for this article.)

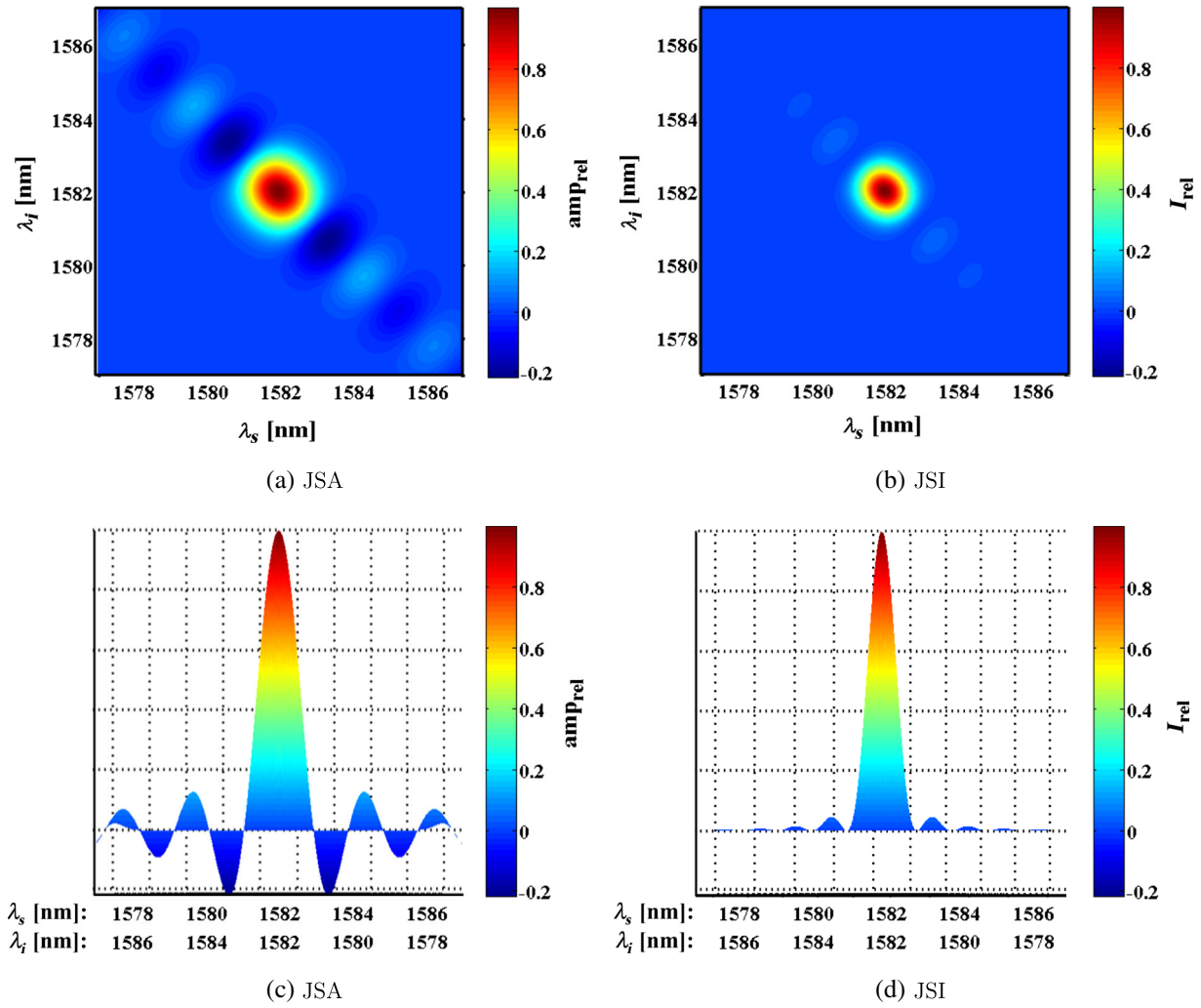

(a) JSA (b) JSI

(c) JSA (d) JSI

FIG. 3. Spectral distribution of a frequency-degenerate type-II SPDC, 791 nm(o) → 1582 nm(o) + 1582 nm(e), in a 30-mm PPKTP using a 2.5-ps pump. Although the main peak is entirely frequency uncorrelated, the purity is still limited ($P \sim 0.83$, $K \sim 1.2$) due to the sidelobes in the joint spectral amplitude (a). In the joint spectral intensity distribution (b), however, the sidelobes are suppressed by a squaring of the JSA, resulting in a very low Schmidt number, $K_{\mathrm{JSI}} \sim 1.01$. (c),(d) Diagonal cross sections of the 3D representations of (a) and (b), respectively.

intrinsic purity of $P > 0.96$. However, this configuration does not allow for spectral indistinguishability (even when the center wavelengths are the same) since the pump amplitude μ and ψ will never intersect orthogonally, which will result in unequal signal and idler bandwidths. While $D = 1$ is preferred for multiphoton experiments, GVM with $D = 0$ is clearly favorable for heralded-photon sources where spectral indistinguishability between signal and idler is not a requirement.

The two types of group-velocity matching are illustrated via examples in Fig. 1. Figures 1(a), 1(b), and 1(c) correspond to the type-II down-conversion 791 nm(o) → 1582 nm(o) + 1582 nm(e) in PPKTP with $D = -(6.027\ \mathrm{ps/mm} - 5.880\ \mathrm{ps/mm})/(6.027\ \mathrm{ps/mm} - 6.175\ \mathrm{ps/mm}) = 0.993$. This configuration generates fully spectrally indistinguishable photons with a compromised purity of, maximally, $P \sim 0.83$. Figures 1(d), 1(e), and 1(f) correspond to the process 612 nm(o) → 1224 nm(o) + 1224 nm(e) in PPKTP with $D = -(6.209\ \mathrm{ps/mm} - 6.208\ \mathrm{ps/mm})/(6.209\ \mathrm{ps/mm} - 5.903\ \mathrm{ps/mm}) = -0.003$ and a purity of $P \sim 0.96$. Owing to the differing bandwidths, signal and idler are easily distinguishable, which is a drawback for multiphoton experiments but is irrelevant for heralding purposes.

Designing an experimental setup that generates photons of high intrinsic purity is only possible in specific configurations of wavelengths, polarizations, and nonlinear crystal, where either $D \sim 0$ or $D \sim 1$. In addition, once such a configuration is found, the length of the crystal has to be matched to the spectral bandwidth of the pump laser (especially for the case $D \sim 1$), as illustrated in Fig. 2. A long crystal combined with a broadband laser will generate

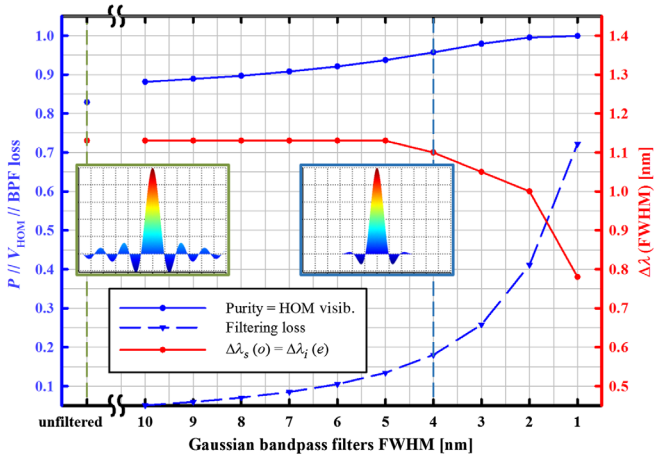

FIG. 4. The effects of bandpass filtering at frequency-degenerate type-II SPDC, 791 nm$(o) \rightarrow 1582$ nm$(o) + 1582$ nm(e), in a 30-mm PPKTP using a 2.5-ps pump. The x axis represents the full width at half maximum (FWHM) of Gaussian bandpass filters in the signal and idler channel. The solid blue line represents the spectral purity P which coincides with the Hong-Ou-Mandel visibility V_{HOM} since, for this setup, signal and idler are spectrally indistinguishable ($\lambda_s = \lambda_i$, $\Delta\lambda_s = \Delta\lambda_i$, $\Delta = 0$). The intensity losses due to filtering are illustrated by the dashed blue line. The red line indicates the FWHM of the filtered photons. The left inset depicts the JSA of the unfiltered case ($P \sim 0.83$); the right inset illustrates the JSA under 4 nm-bandpass filtering. The vertical dashed sky-blue line indicates that the purity can be improved to $P > 0.95$ under intensity losses of less than 20%.

frequency-correlated daughter photons. Conversely, a short crystal and narrow-bandwidth laser will result in anticorrelated spectra. Both cases undermine the purity of the generated photon states.

Even in cases where the experimentally observed spectral distribution of signal and idler is almost uncorrelated ($K_{\mathrm{JSI}} \leq 1.01$), interference visibilities might still be undermined due to correlations in the JSA [41]. These spectral correlations are introduced by sidelobes in the JSA, caused by the sinc function in the QPM amplitude ψ. These sidelobes are suppressed in the JSI by a squaring of the JSA, as depicted in Fig. 3. Although the actual HOM visibility depends on the factorability of the JSA, it nonetheless makes sense to pay attention to K_{JSI} as well since a low Schmidt number of $K_{\mathrm{JSI}} \leq 1.01$ indicates that the main peak of the joint spectral distribution is factorable and the purity is undermined by the sidelobes only. These sidelobes, however, can be removed by bandpass filtering under a relatively low intensity loss, as illustrated by the example in Fig. 4. In this example, identical Gaussian-shape bandpass filters with ideal transmission (100%) on each photon are considered for a particular QPM process, i.e., 791 nm$(o) \rightarrow 1582$ nm$(o) + 1582$ nm(e). As shown in the plot, the purity extracted from the HOM visibility between independent photons increases by cutting the sidelobes of the joint spectrum through the filters while introducing a reasonable amount of loss, and therefore maintaining high count rates. While, for this example, we assumed identical filters in each of the four arms of two SPDC sources, we showed previously that two out of four possible filters were already able to enhance the purity substantially [42]. In the remainder of this article, we speak of "intrinsically pure" SPDC when $K_{\mathrm{JSI}} \leq 1.01$—hence, when high purity can be achieved without or with very low-loss filtering.

Note that the simulations in this article do not include a study of the spatial correlations between the

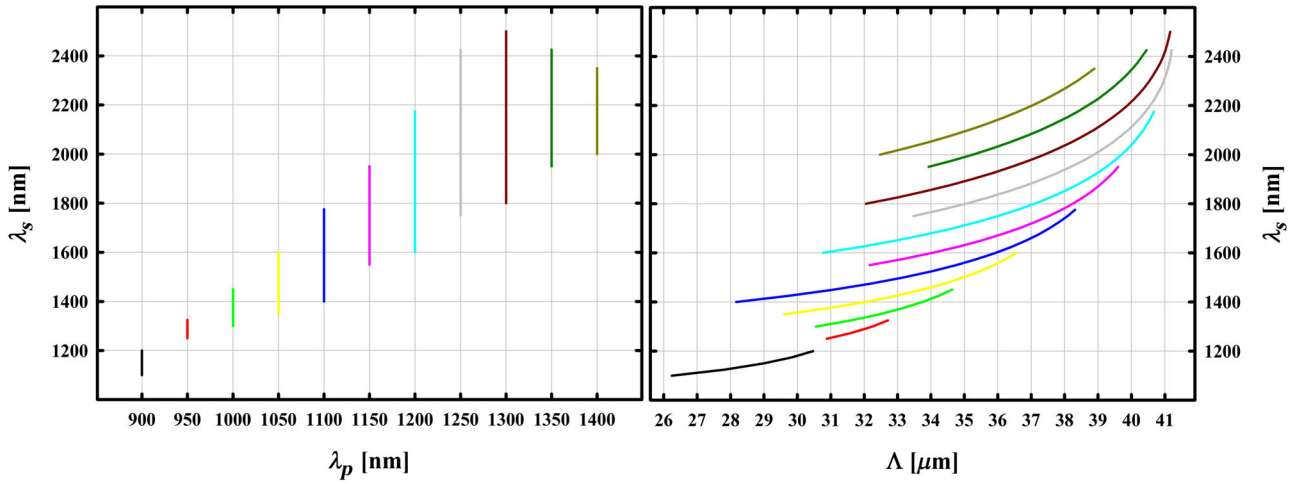

FIG. 5. Signal wavelength versus (left panel) pump wavelength λ_p and (right panel) crystal periodicity Λ for pure type-0 SPDC ($e \rightarrow e + e$) in PPKTP ($d_{\mathrm{eff}} \sim 9.5$ pm V^{-1}). The plots display configurations which allow for spectrally uncorrelated signal- and idler-photon states under no or low-loss bandpass filtering. Each colored line corresponds to a particular pump wavelength λ_p and depicts the range of signal wavelength over which a Schmidt number of $K_{\mathrm{JSI}} \leq 1.01$ can be achieved by the mutual matching of pump spectrum and crystal length. Note that all depicted data correspond to a crystal temperature of 50 °C and is slightly modified with varying temperature. (This figure was previously published in Ref. [3].)

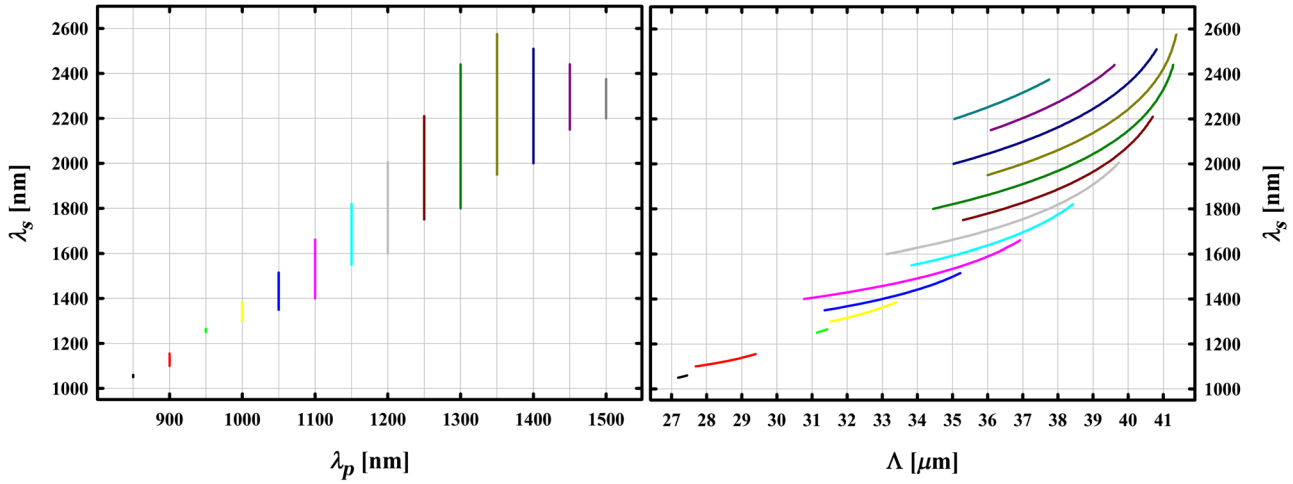

FIG. 6. Signal wavelength versus (left panel) pump wavelength λ_p and (right panel) crystal periodicity Λ for pure type-0 SPDC ($e \rightarrow e + e$) in PPCTA ($d_{\text{eff}} \sim 11.2$ pm V^{-1}).

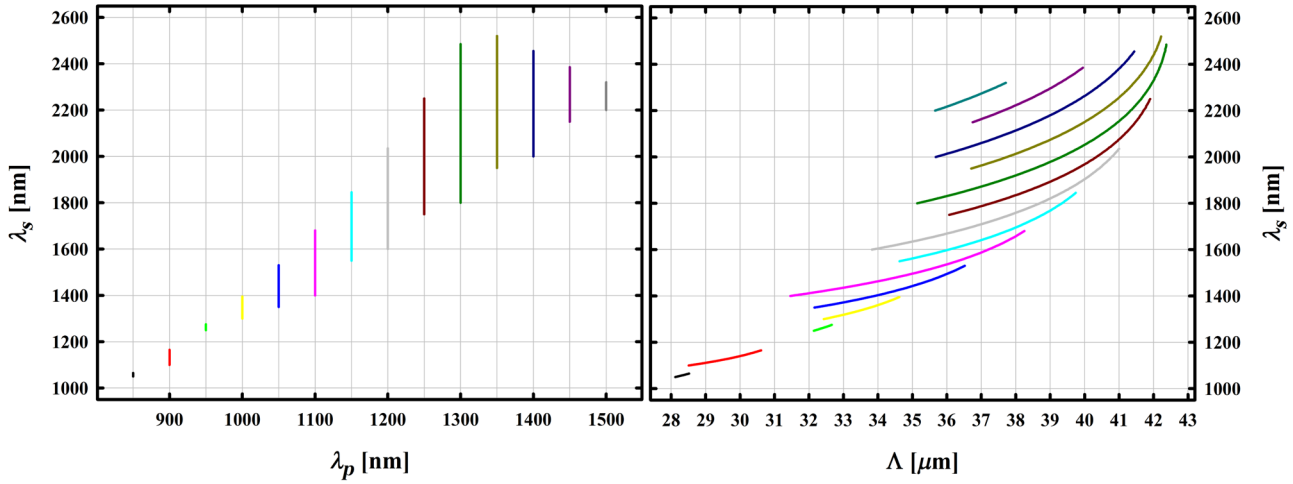

FIG. 7. Signal wavelength versus (left panel) pump wavelength λ_p and (right panel) crystal periodicity Λ for pure type-0 SPDC ($e \rightarrow e + e$) in PPKTA ($d_{\text{eff}} \sim 9.6$ pm V^{-1}).

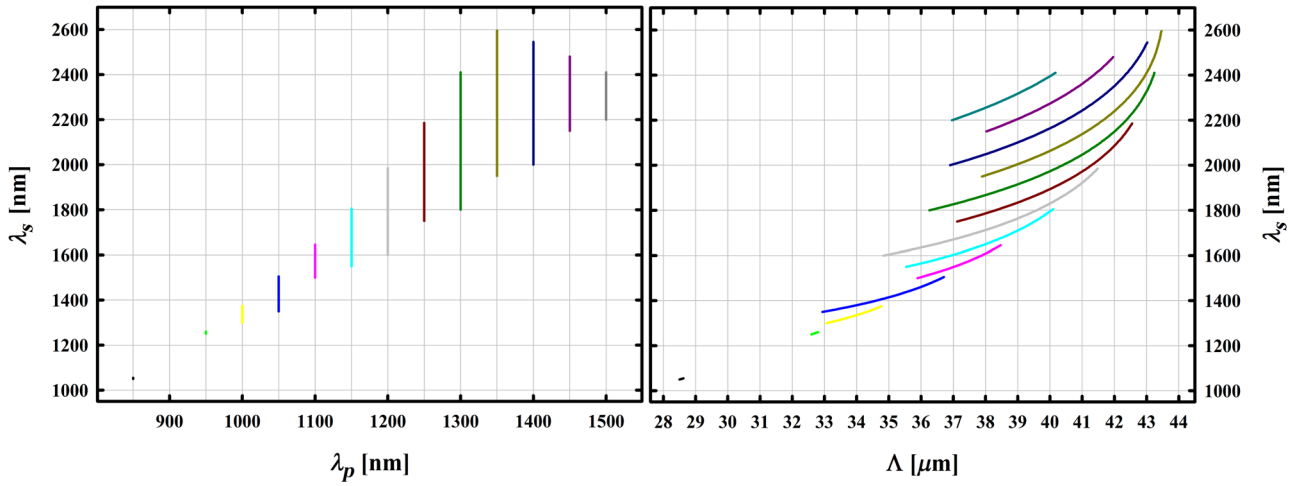

FIG. 8. Signal wavelength versus (left panel) pump wavelength λ_p and (right panel) crystal periodicity Λ for pure type-0 SPDC ($e \rightarrow e + e$) in PPRTA ($d_{\text{eff}} \sim 9.8$ pm V^{-1}).

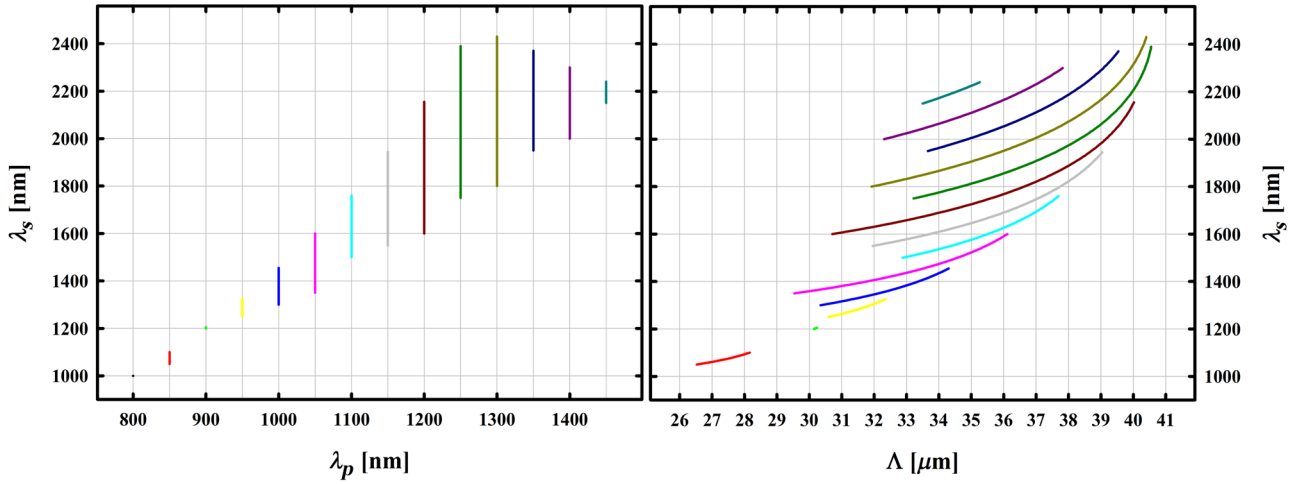

FIG. 9. Signal wavelength versus (left panel) pump wavelength λ_p and (right panel) crystal periodicity Λ for pure type-0 SPDC ($e \rightarrow e + e$) in PPRTP ($d_{\text{eff}} \sim 9.6$ pm V^{-1}).

down-converted photons. These correlations become relevant when the photons are collected via single-mode fibers in order to be processed and detected. Taking the spatial correlations into account [2,40,43–45], it is possible to cut the sidelobes of the JSA directly through spatial filtering of the single-mode coupling: Assuming the pump beam has a large waist at the center of the crystal, one can find the specific configuration of single-mode fibers and coupling lenses for which the spatial correlations increase and the frequency correlations reduce. Increasing the beam waist decreases the total coupling efficiency and, therefore, in a similar way to the bandpass-filtering approach, one should find the optimal design for high purity and count rates as required by the experiment.

This section provides a collection and discussion of configurations in which uncorrelated spectra can, in principle, be achieved—provided a matched laser bandwidth and crystal length. The calculations are based on the dispersion equations and other material properties of KTP, CTA, KTA, RTA, and RTP [46–52]. Note that only type-0 and type-II down-conversion is mentioned since, according to our calculations, KTP and its isomorphs do not allow for intrinsically pure states at type-I SPDC (signal and idler parallelly polarized, but orthogonally with respect to the pump). However, pure states generated by type-I down-conversion are possible using periodically poled lithium niobate and lithium tantalate [3].

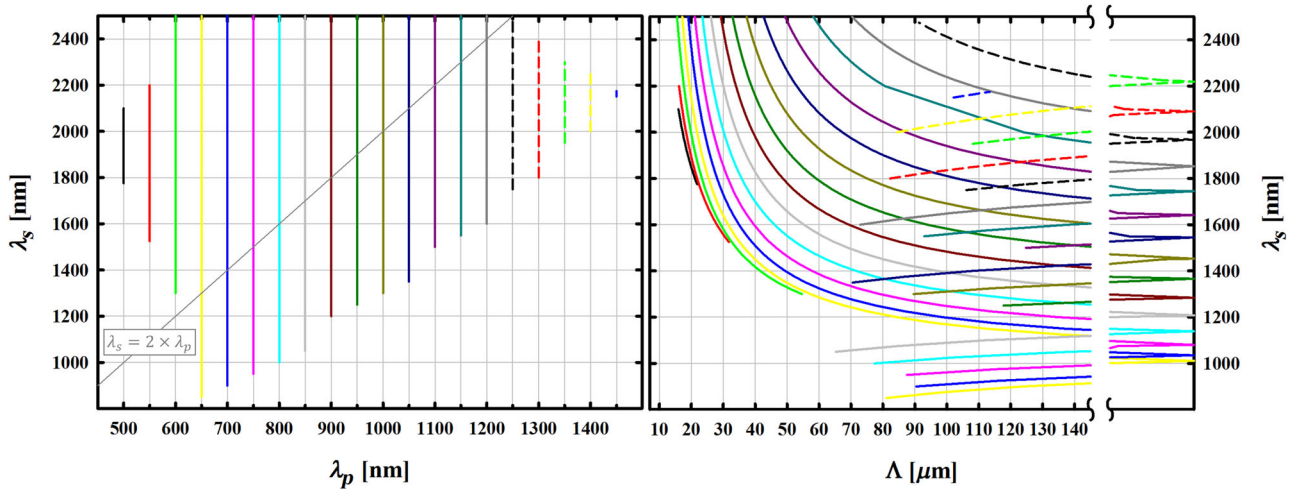

FIG. 10. Signal wavelength versus (left panel) pump wavelength λ_p and (right panel) crystal periodicity Λ for high intrinsic purity at type-II SPDC ($o \rightarrow o + e$) in PPKTP ($d_{\text{eff}} = d^{32} \sim 2.4$ pm V^{-1}) at $T = 50\,^{\circ}$C. The gray line in the left plot represents spectrally symmetric down-conversions. The right plot indicates a range of pump and signal wavelengths for which the periodicity Λ approaches infinity, thus enabling spectrally pure output generation without periodic poling (displayed in Figs. 17 and 18). (A similar figure was previously published in Ref. [3] and was modified for this article.)

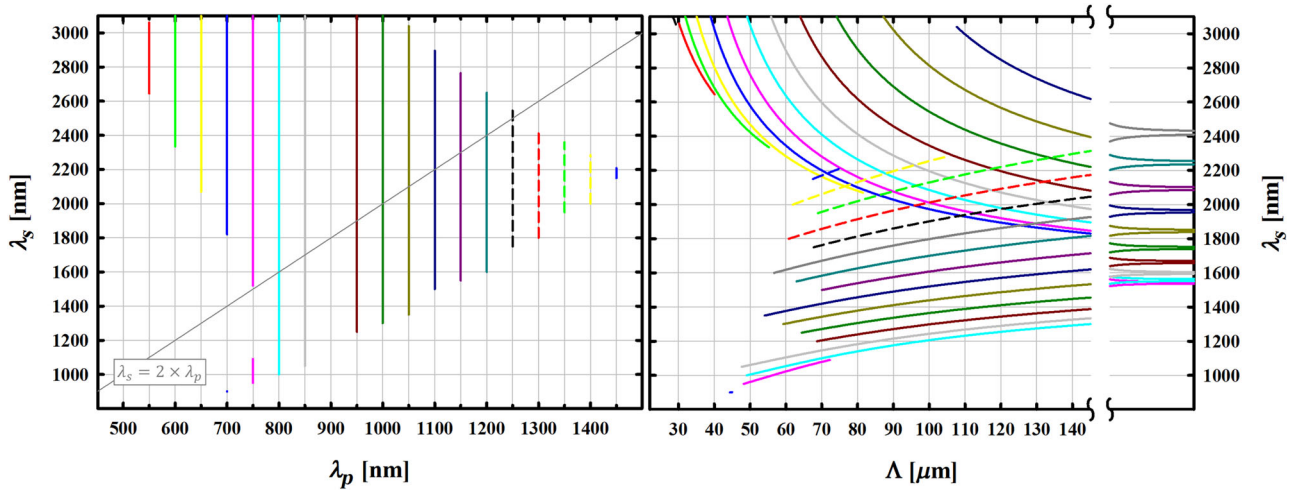

FIG. 11. Signal wavelength versus (left panel) pump wavelength λ_p and (right panel) crystal periodicity Λ for high intrinsic purity at type-II SPDC ($o \rightarrow o + e$) in PPCTA ($d_{\text{eff}} = d^{32} \sim 2.1$ pm V^{-1}).

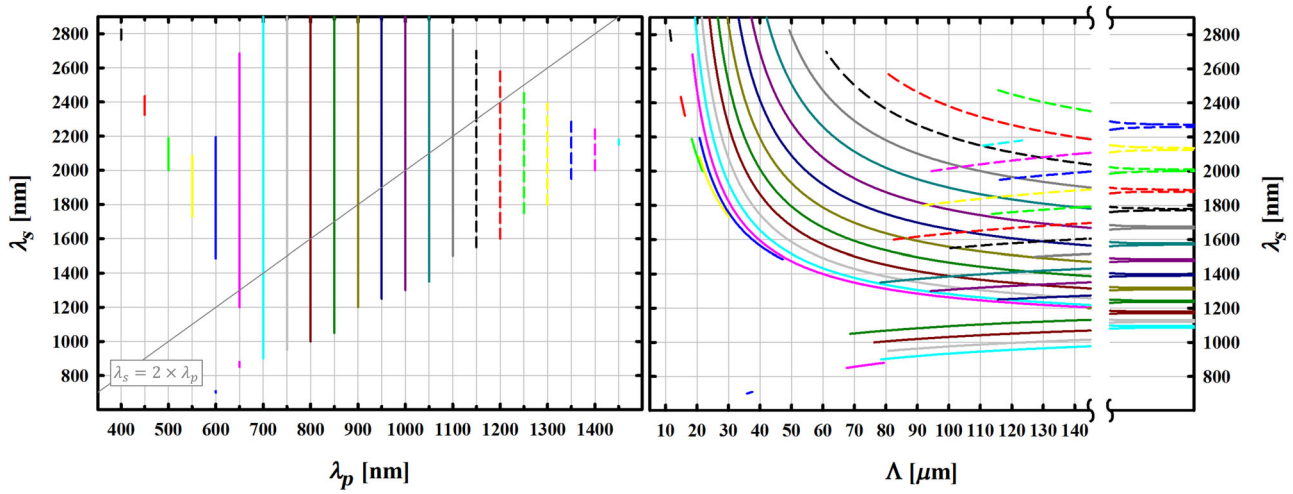

FIG. 12. Signal wavelength versus (left panel) pump wavelength λ_p and (right panel) crystal periodicity Λ for high intrinsic purity at type-II SPDC ($o \rightarrow o + e$) in PPKTA ($d_{\text{eff}} = d^{32} \sim 2.3$ pm V^{-1}).

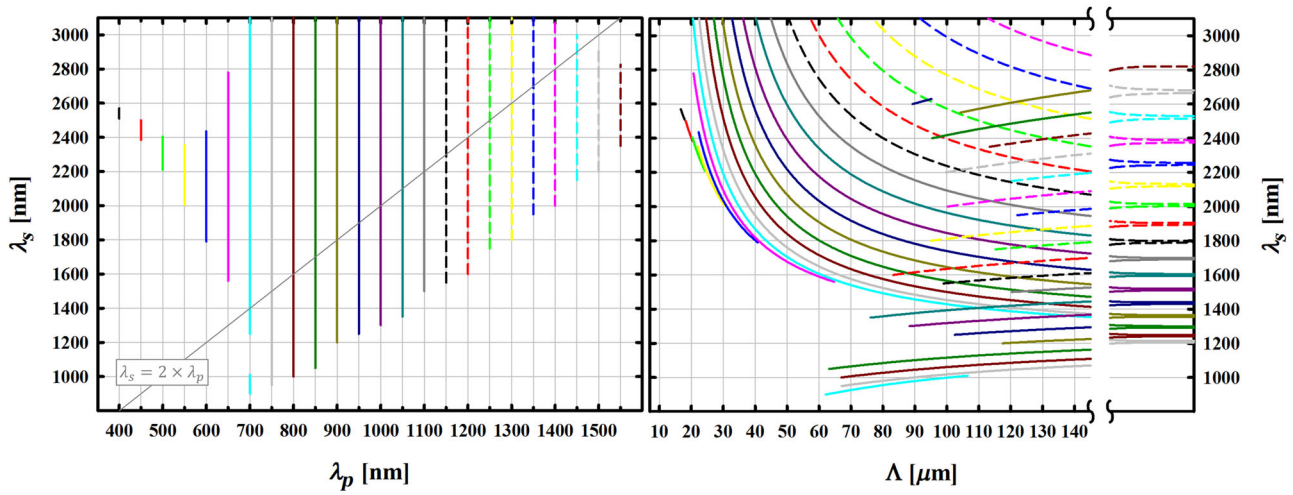

FIG. 13. Signal wavelength versus (left panel) pump wavelength λ_p and (right panel) crystal periodicity Λ for high intrinsic purity at type-II SPDC ($o \rightarrow o + e$) in PPRTA ($d_{\text{eff}} = d^{32} \sim 2.4$ pm V^{-1}).

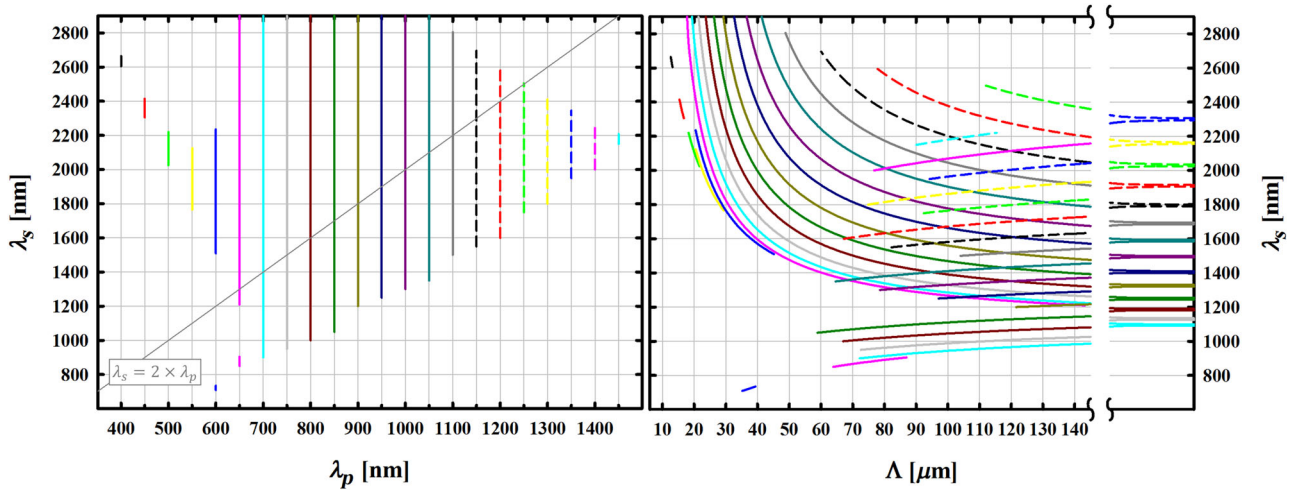

FIG. 14. Signal wavelength versus (left panel) pump wavelength λ_p and (right panel) crystal periodicity Λ for high intrinsic purity at type-II SPDC ($o \to o + e$) in PPRTP ($d_{\text{eff}} = d^{32} \sim 2.4\ \text{pm}\,\text{V}^{-1}$).

A. Type 0

When signal and idler are not required to be orthogonally polarized (i.e., in nondegenerate SPDC processes), type-0 down-conversion is often preferred over other polarization configurations due to higher effective nonlinearities, and hence greater pair-generation rates. Figures 5–9 describe type-0 SPDC processes which allow for high intrinsic purity when the crystal length and pump pulse duration are mutually matched. The plots on the left-hand side depict pump- and signal-wavelength combinations for which a Schmidt number K_{JSI} smaller than or equal to 1.01 is possible. The plots on the right-hand side illustrate the very same states (with each color representing a particular pump wavelength), but with respect to the poling period Λ of the nonlinear crystal. Unfortunately, as the plots illustrate, high intrinsic purity at type-0 SPDC is possible only in rather unfavorable wavelength configurations where the signal and/or idler photon is too long waved to be processed and detected efficiently.

B. Type II

Many experiments require photon pairs of orthogonal polarization, allowing, e.g., for an easy separation of the pairs into different spatial modes and generation of polarization entanglement. Find in this section a collection of intrinsically pure type-II down-conversion states, depicted in Fig. 10–14. The gray line in the left graphs represents the important special case of frequency-degenerate down-conversion. These configurations are more deeply investigated, in terms of purity and indistinguishability, in Sec. III B 1. The plots on the right side indicate that, for all five materials, there is a set of wavelength configurations for which the required poling period approaches infinity. This interesting feature allows for collinear and intrinsically pure SPDC in *bulk* crystals with no periodic poling required (see Sec. III B 2 for a closer investigation).

1. Frequency-degenerate SPDC

Photon pairs with the same center wavelength but orthogonal polarization find many applications in quantum optics. As illustrated in the previous section, each crystal comes with a large set of possible spectrally pure and frequency-degenerate SPDC states. However, there is for each material only one point where the exact same center wavelength *and* spectral bandwidth can be achieved—hence, where the dispersion parameter D [Eq. (9)] equals 1.

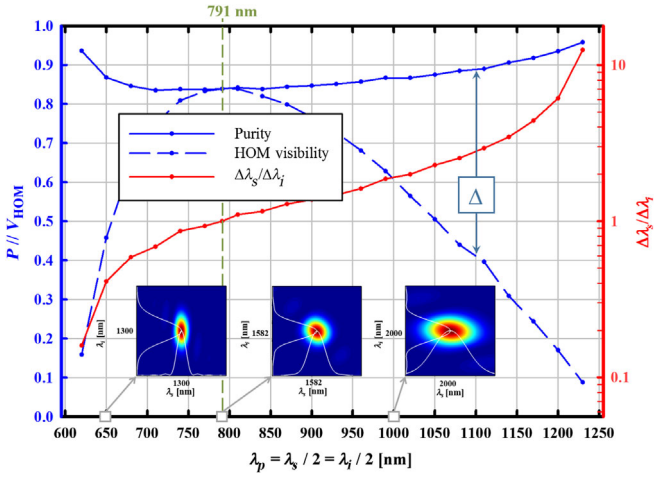

FIG. 15. Intrinsically pure frequency-degenerate type-II SPDC states with PPKTP. For each pump wavelength on the x axis, the crystal length and the pump bandwidth are mutually matched to maximize the purity. The solid blue line represents the maximally achievable spectral purity P, whereas the dashed blue line depicts the HOM visibility $V_{\text{HOM}} = P - \Delta$, where Δ is a measure for spectral distinguishability. The red line represents the ratio of signal-to-idler bandwidth. Maximal spectral indistinguishability can be achieved at $\lambda_p = 791$ nm, as indicated by $\Delta\lambda_s/\Delta\lambda_i = 1$ and the intersection of the blue lines ($P = V_{\text{HOM}}$). (A similar figure was previously published in Ref. [3] and has been modified for this article.)

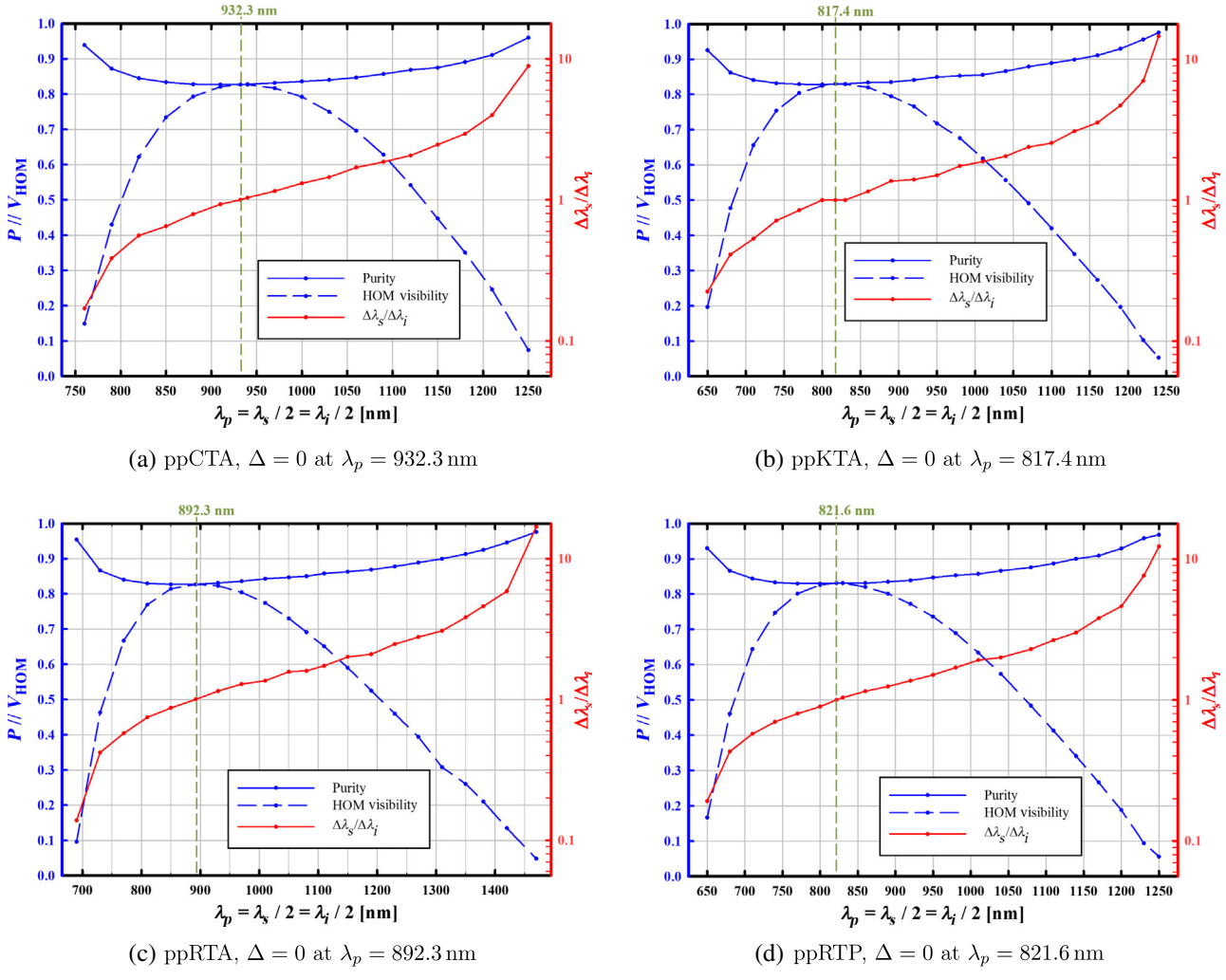

(a) ppCTA, $\Delta = 0$ at $\lambda_p = 932.3\,\mathrm{nm}$

(b) ppKTA, $\Delta = 0$ at $\lambda_p = 817.4\,\mathrm{nm}$

(c) ppRTA, $\Delta = 0$ at $\lambda_p = 892.3\,\mathrm{nm}$

(d) ppRTP, $\Delta = 0$ at $\lambda_p = 821.6\,\mathrm{nm}$

FIG. 16. Intrinsically pure frequency-degenerate type-II SPDC with (a) PPCTA, (b) PPKTA, (c) PPRTA, and (d) PPRTP.

These configurations of maximal spectral indistinguishability can be regarded as material constants of the respective nonlinear crystals. Figures 15 and 16 depict the maximally achievable purity and HOM visibility for frequency-degenerate down-conversion with respect to the pump wavelength. The graphs illustrate that minimal indistinguishability Δ does not correspond to maximal spectral purity P. This is due to the spectral correlations carried by the sidelobes of the sinc function in the QPM amplitude.

2. Pure states without periodic poling

As indicated by Figs. 10–14, for each of the investigated materials there is a domain where intrinsically pure type-II SPDC can be achieved with crystals of the infinite poling period Λ, i.e., for crystals which are not periodically poled at all. This pecularity brings of course the advantage of cost-efficient experimental solutions since the elaborate manufacturing of ferroelectric poling in micrometer domains becomes obsolete. The possible configurations allowing for this approach are depicted in Figs. 17 and 18.

For most setups the accessible signal and/or idler wavelengths are beyond 2 μm, a regime which is—while invisible for up-to-date Si or InGaAs photodiodes—currently approached by superconducting nanowire detectors [53,54]. However, as illustrated in Fig. 17, CTA makes up a pleasant exception: According to our simulations, bulk (hence not periodically poled) CTA allows for the generation of intrinsically pure and frequency-degenerate type-II SPDC in the popular telecom regime $775\ \mathrm{nm}(o) \rightarrow 1550\ \mathrm{nm}(o) + 1550\ \mathrm{nm}(e)$.

IV. INTRINSIC ENTANGLEMENT

Until very recently, the generation of entangled photon pairs using collinear SPDC required an elaborate setup, involving at least two superimposed beam paths [21–30] or a periodically poled crystal with alternating poling periodicities [55,56]. In our recent paper [20], we demonstrated

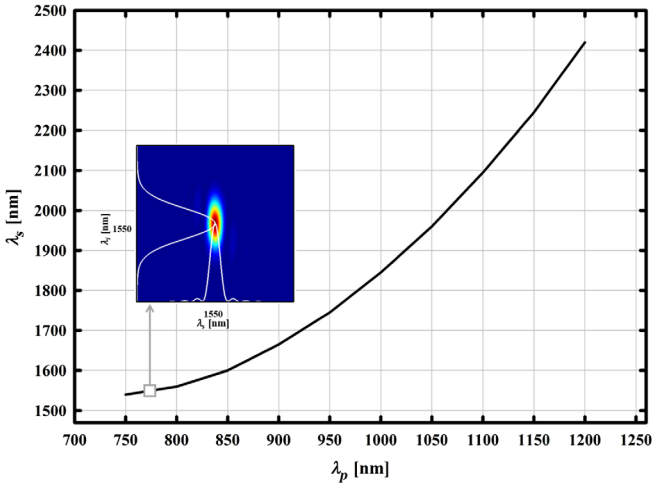

FIG. 17. Pure states with bulk CTA, $o \rightarrow o + e$. Illustration of setups for type-II SPDC which allow for phase-matched and intrinsically pure states in bulk—not periodically poled—CTA. The idler wavelength corresponding to a pair of λ_p and λ_s is obtained by energy conservation. The inset corresponds to a collinear down-conversion from 775 nm to 2 times 1550 nm in a CTA crystal without periodic ferroelectric poling and with a purity of $P \sim 0.91$.

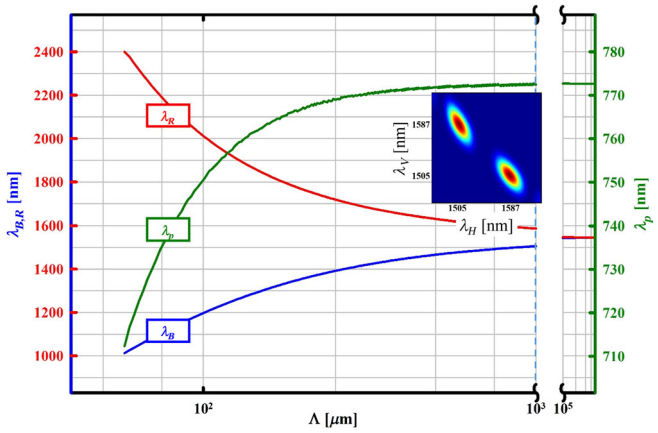

FIG. 19. PPCTA, $o \rightarrow o + e$, intrinsic entanglement. Possible configurations allowing for the intrinsic entanglement of photons generated by CDDC in PPCTA. The blue and red lines represent the short- and long-wave photons, respectively (each coming in both polarizations H and V); the green line represents the wavelength of the pump laser. With increasing crystal periodicity Λ the wavelengths λ_B and λ_R are approaching each other which gives rise to the opportunity of creating photon pairs with similar bandwidths and group velocities. The vertical dashed light-blue line and the inset represent the down-conversion 772.5 nm$(o) \rightarrow$ 1505 nm$(o, e) +$ 1587 nm(e, o), which is not only of interest due to the telecom wavelengths but also due to similar bandwidths and group delay in the crystal, allowing for high entanglement visibility and brightness (since no bandpass filtering is required).

an alternative method to generate photonic frequency and polarization entanglement, using only one unidirectionally pumped crystal, with a uniform poling period. Our method is based on the fact that a periodically poled nonlinear crystal with grating constant Λ, pumped by a laser with center wavelength λ_p, can provide phase matching for two different SPDC processes simultaneously, referred to as CDDC. The poling period required to support a given down-conversion configuration obeys

$$\Lambda = m\frac{2\pi}{\Delta k} = m\frac{2\pi}{k_p - k_s - k_i}. \tag{11}$$

In principle, two different pairs of signal and idler wavelength $\lambda_{s1}, \lambda_{i1}$ and $\lambda_{s2}, \lambda_{i2}$ can yield a momentum difference Δk of equal magnitude but opposite sign. This will, according to the above equation, lead to the same periodicity Λ, with, however, one SPDC process exploiting the QPM order $m = 1$ and another $m = -1$. Now, under careful choice of experimental parameters, two

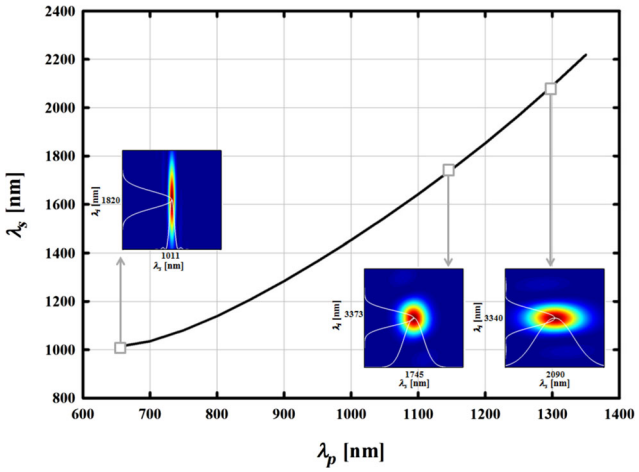

(a) KTP

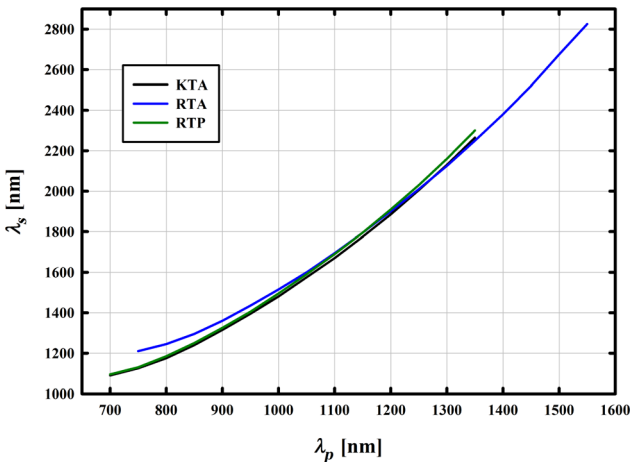

(b) KTA, RTA, RTP

FIG. 18. Pure type-II SPDC states with bulk (a) KTP and (b) KTA, RTA, and RTP. [(a) was previously published in Ref. [3]].

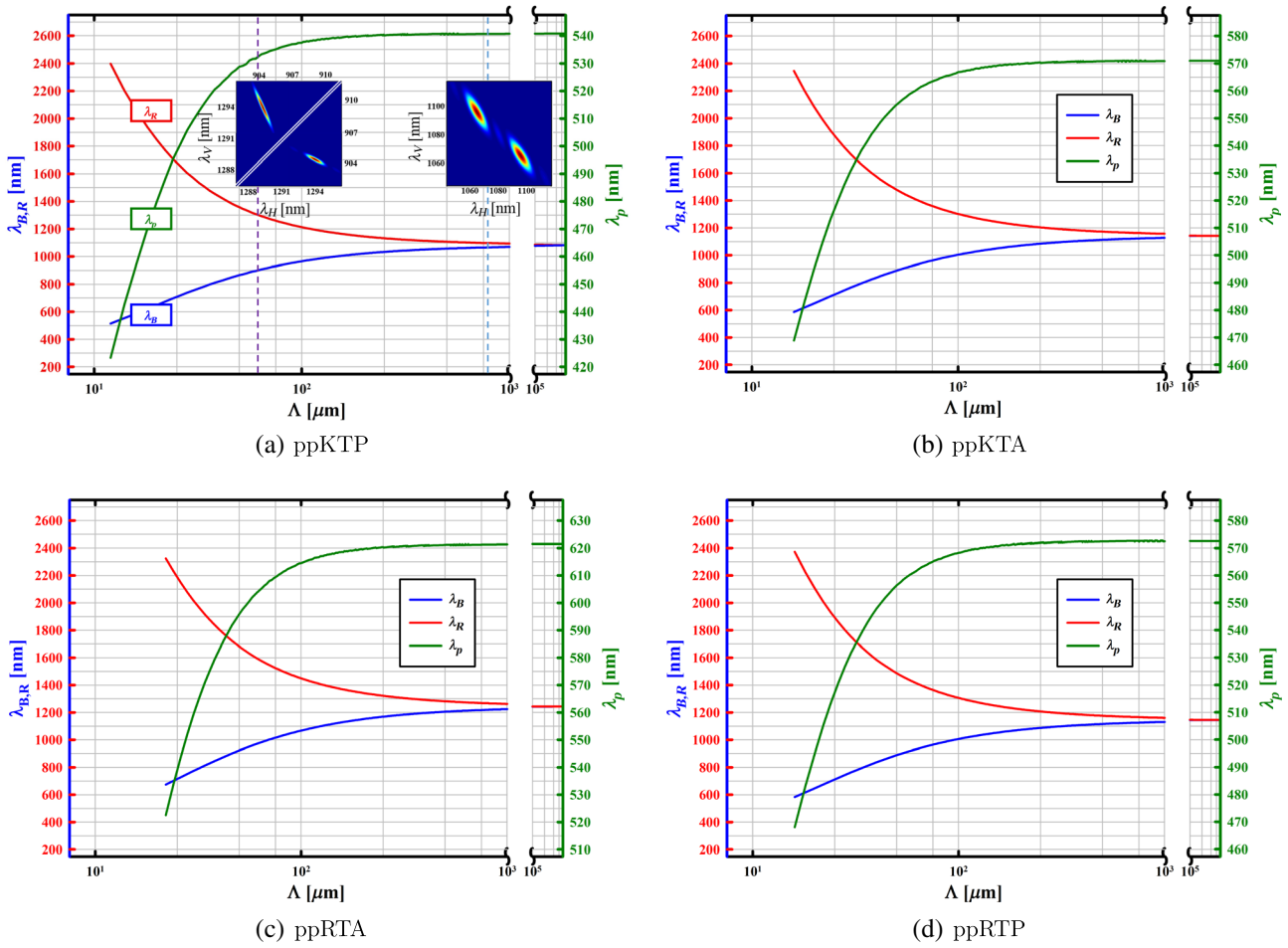

FIG. 20. Possible wavelength configurations for intrinsic-entanglement generation in (a) PPKTP, (b) PPKTA, (c) PPRTA, and (d) PPRTP. The vertical dashed purple line and the corresponding inset graph in (a) highlight the first experimental demonstration $\lambda_{p0} = 532.3$ nm, $\lambda_B = 904.3$ nm and $\lambda_R = 1293.9$ nm in PPKTP. The right inset graph over the vertical dashed light-blue line represents a configuration with similar bandwidth and group velocities. However, as these wavelengths lie at around 1.1 μm, they are difficult to detect with commonly used Si or InGaAs detectors—a drawback which can be overcome by using PPCTA, as seen in Fig. 19. [(a) was previously published in Ref. [20].]

simultaneous down-conversion processes can generate photon pairs with coinciding wavelengths but opposite polarization:

$$\lambda_{H1}(m=1) = \lambda_{V2}(m=-1), \tag{12a}$$

$$\lambda_{V1}(m=1) = \lambda_{H2}(m=-1), \tag{12b}$$

where the corresponding wave numbers $k = 2\pi n/\lambda$ fulfill the relation

$$k_{H1} + k_{V1} = -(k_{H2} + k_{V2}). \tag{13}$$

Considering that, in each pair, one photon is short waved (blue, B) and the other one long waved (red, R), we obtain the polarization- and wavelength-entangled state

$$\begin{aligned}|\Psi\rangle &= \alpha \hat{a}^\dagger_{HB}\hat{a}^\dagger_{VR}|0\rangle + \beta \hat{a}^\dagger_{HR}\hat{a}^\dagger_{VB}|0\rangle \\ &=: \alpha|HV\rangle \otimes |BR\rangle + \beta|HV\rangle \otimes |RB\rangle,\end{aligned} \tag{14}$$

which was successfully experimentally demonstrated in Ref. [20]. This method is however only usable with particular nonlinear crystals, each supporting a finite set of possible wavelength configurations. Figures 19 and 20 illustrate possible experimental realizations of inherent-entanglement generation in the family of KTP-isomorphic crystals. For each poling period Λ on the x axis, there is one given pump wavelength λ_p which generates daughter photons with wavelengths λ_B and λ_R, each coming in horizontal and vertical polarization. The graphs show that, for long periods Λ, the signal and idler wavelengths become more and more similar. This feature is beneficial for the entanglement visibility since relative differences of the group delays due to wavelength dispersion become

negligible. Furthermore, the left inset in Fig. 20(a) illustrates that, for a smaller Λ, the two SPDC processes generate photons with interchangeable center wavelengths but different spectral bandwidths. This introduces a certain degree of spectral distinguishability which undermines the entanglement visibility, an impairment which can be overcome by insertion of a bandpass filter in one channel. However, as suggested by the insets in Figs. 19 and 20(a), for larger periods Λ, the bandwidths become very similar, therefore allowing for high indistinguishability even without bandpass filtering.

It turns out that, as illustrated in Fig. 19, the material PPCTA offers a convenient opportunity to generate entangled photons with similar bandwidth (and hence no filtering required) and low relative group delay $[(\Delta\mathrm{GD})_{si} \approx 0.2\ \mathrm{ps/mm}]$ with both photons in the telecom band.

V. CONCLUSION

In this paper, we present a profound numerical evaluation of five nonlinear materials, KTP, CTA, KTA, RTA, and RTP, as well as the opportunities they offer in terms of spectrally pure down-conversion states and entanglement generation. Specifically, we find that CTA allows for the generation of collinear photon pairs with a degenerate telecom wavelength of 1550 nm, orthogonal polarization, and high spectral purity at the same time—all without the need for ferroelectric periodic poling. As a second remarkable feature of this material, we show that periodically poled CTA can be used for the compact and efficient generation of polarization- and frequency-entangled photon pairs with high visibility in the telecom regime. In addition, we numerically investigate the relation of purity and Hong-Ou-Mandel visibility and model the effects of bandpass filtering in terms of intensity loss and quantum performance.

We believe that this work can be a helpful resource to any experimentalist who uses periodically poled nonlinear crystals in order to generate highly performing photon pairs. We hope that this article will act as an incentive to further investigate and manufacture the more exotic nonlinear materials CTA, KTA, RTA, and RTP.

ACKNOWLEDGMENTS

This work was funded by the Austrian Research Promotion Agency (Österreichische Forschungsförderungsgesellschaft, FFG) through KVQ (Grant No. 4642983). C. G. and P. W. acknowledge support from the European Commission through EQUAM (Grant No. 323714), PICQUE (Grant No. 608062), and QUCHIP (Grant No. 641039), as well as from the Austrian Science Fund (FWF) through START (Grant No. Y585-N20), CoQuS (Grant No. W1210-4), and NaMuG (Grant No. P30067-N36).

[1] E. Meyer-Scott, N. Montaut, J. Tiedau, L. Sansoni, H. Herrmann, T. J. Bartley, and C. Silberhorn, Limits on the heralding efficiencies and spectral purities of spectrally filtered single photons from photon-pair sources, Phys. Rev. A **95**, 061803(R) (2017).

[2] T. Guerreiro, A. Martin, B. Sanguinetti, N. Bruno, H. Zbinden, and R. T. Thew, High efficiency coupling of photon pairs in practice, Opt. Express **21**, 27641 (2013).

[3] F. Laudenbach, H. Hübel, M. Hentschel, P. Walther, and A. Poppe, Modelling parametric down-conversion yielding spectrally pure photon pairs, Opt. Express **24**, 2712 (2016).

[4] P. J. Mosley, J. S. Lundeen, B. J. Smith, and I. A. Walmsley, Conditional preparation of single photons using parametric downconversion: A recipe for purity, New J. Phys. **10**, 093011 (2008).

[5] A. B. U'Ren, C. Silberhorn, R. Erdmann, K. Banaszek, W. P. Grice, I. A. Walmsley, and M. G. Raymer, Generation of pure-state single-photon wavepackets by conditional preparation based on spontaneous parametric downconversion, Laser Phys. **15**, 146 (2005).

[6] R.-B. Jin, R. Shimizu, K. Wakui, H. Benichi, and M Sasaki, Widely tunable single photon source with high purity at telecom wavelength, Opt. Express **21**, 10659 (2013).

[7] P. G. Evans, R. S. Bennink, W. P. Grice, T. S. Humble, and J. Schaake, Bright Source of Spectrally Uncorrelated Polarization-Entangled Photons with Nearly Single-Mode Emission, Phys. Rev. Lett. **105**, 253601 (2010).

[8] A. Eckstein, A. Christ, P. J. Mosley, and C. Silberhorn, Highly Efficient Single-Pass Source of Pulsed Single-Mode Twin Beams of Light, Phys. Rev. Lett. **106**, 013603 (2011).

[9] K. Edamatsu, R. Shimizu, W. Ueno, R.-B. Jin, F. Kaneda, M. Yabuno, H. Suzuki, S. Nagano, A. Syouji, and K. Suizu, Photon pair sources with controlled frequency correlation, Progr. Informat. **8**, 19 (2011).

[10] M. Yabuno, R. Shimizu, Y. Mitsumori, H. Kosaka, and K. Edamatsu, Four-photon quantum interferometry at a telecom wavelength, Phys. Rev. A **86**, 010302 (2012).

[11] R.-B. Jin, K. Wakui, R. Shimizu, H. Benichi, S. Miki, T. Yamashita, H. Terai, Z. Wang, M. Fujiwara, and M. Sasaki, Nonclassical interference between independent intrinsically pure single photons at telecommunication wavelength, Phys. Rev. A **87**, 063801 (2013).

[12] R.-B. Jin, R. Shimizu, I. Morohashi, K. Wakui, M. Takeoka, S. Izumi, T. Sakamoto, M. Fujiwara, T. Yamashita, S. Miki, H. Terai, Z. Whang, and M. Sasaki, Efficient generation of twin photons at telecom wavelengths with 2.5 GHz repetition-rate-tunable comb laser, Sci. Rep. **4**, 7468 (2014).

[13] M. M. Weston, H. M. Chrzanowski, S. Wollmann, A. Boston, J. Ho, L. K. Shalm, V. B. Verma, M. S. Allman, S. W. Nam, R. B. Patel, S. Slussarenko, and G. J. Pryde, Efficient and pure femtosecond-pulse-length source of polarization-entangled photons, Opt. Express **24**, 10869 (2016).

[14] W. P. Grice, A. B. U'ren, and I. A. Walmsley, Eliminating frequency and space-time correlations in multiphoton states, Phys. Rev. A **64**, 063815 (2001).

[15] P. J. Mosley, J. S. Lundeen, B. J. Smith, P. Wasylczyk, A. B. U'Ren, C. Silberhorn, and I. A. Walmsley, Heralded Generation of Ultrafast Single Photons in Pure Quantum States, Phys. Rev. Lett. **100**, 133601 (2008).

[16] P. B. Dixon, J. H. Shapiro, and F. N. C. Wong, Spectral engineering by Gaussian phase-matching for quantum photonics, Opt. Express **21**, 5879 (2013).

[17] A. Dosseva, Ł. Cincio, and A. M. Brańczyk, Shaping the joint spectrum of down-converted photons through optimized custom poling, Phys. Rev. A **93**, 013801 (2016).

[18] F. Graffitti, D. Kundys, D. T. Reid, A. M. Brańczyk, and A. Fedrizzi, Pure down-conversion photons through sub-coherence-length domain engineering, Quantum Sci. Technol. **2**, 035001 (2017).

[19] C. Chen, C. Bo, M. Y. Niu, F. Xu, Z. Zhang, J. H. Shapiro, and F. N. C. Wong, Efficient generation and characterization of spectrally factorable biphotons, Opt. Express **25**, 7300 (2017).

[20] F. Laudenbach, S. Kalista, M. Hentschel, P. Walther, and H. Hübel, A novel single-crystal & single-pass source for polarisation- and colour-entangled photon pairs, Sci. Rep. **7**, 7235 (2017).

[21] A. Yoshizawa, R. Kaji, and H. Tsuchida, Generation of polarization-entangled photon pairs at 1550 nm using two PPLN waveguides, Electron. Lett. **39**, 621 (2003).

[22] C. Clausen, F. Bussiéres, A. Tiranov, H. Herrmann, C. Silberhorn, W. Sohler, M. Afzelius, and N. Gisin, A source of polarization-entangled photon pairs interfacing quantum memories with telecom photons, New J. Phys. **16**, 093058 (2014).

[23] I. Herbauts, B. Blauensteiner, A. Poppe, T. Jennewein, and H. Huebel, Demonstration of active routing of entanglement in a multi-user network, Opt. Express **21**, 29013 (2013).

[24] M. Pelton, P. Marsden, D. Ljunggren, M. Tengner, A. Karlsson, A. Fragemann, C. Canalias, and F. Laurell, Bright, single-spatial-mode source of frequency non-degenerate, polarization-entangled photon pairs using periodically poled KTP, Opt. Express **12**, 3573 (2004).

[25] H. Hübel, M. R. Vanner, T. Lederer, B. Blauensteiner, T. Lorünser, A. Poppe, and A. Zeilinger, High-fidelity transmission of polarization encoded qubits from an entangled source over 100 km of fiber, Opt. Express **15**, 7853 (2007).

[26] B. S. Shi and A. Tomita, Generation of a pulsed polarization entangled photon pair using a Sagnac interferometer, Phys. Rev. A **69**, 013803 (2004).

[27] F. König, E. J. Mason, F. N. C. Wong, and M. A. Albota, Efficient and spectrally bright source of polarization-entangled photons, Phys. Rev. A **71**, 033805 (2005).

[28] T. Kim, M. Fiorentino, and F. N. C. Wong, Phase-stable source of polarization-entangled photons using a polarization Sagnac interferometer, Phys. Rev. A **73**, 012316 (2006).

[29] A. Fedrizzi, T. Herbst, A. Poppe, T. Jennewein, and A. Zeilinger, A wavelength-tunable fiber-coupled source of narrowband entangled photons, Opt. Express **15**, 15377 (2007).

[30] M. Hentschel, H. Hübel, A. Poppe, and A. Zeilinger, Three-color Sagnac source of polarization-entangled photon pairs, Opt. Express **17**, 23153 (2009).

[31] R. T. Horn, P. Kolenderski, D. Kang, P. Abolghasem, C. Scarcella, A. Della Frera, A. Tosi, L. G. Helt, S. V. Zhukovsky, J. E. Sipe, G. Weihs, A. S. Helmy, and Thomas Jennewein, Inherent polarization entanglement generated from a monolithic semiconductor chip, Sci. Rep. **3**, 2314 (2013).

[32] D. Kang, A. Anirban, and A. S. Helmy, Monolithic semiconductor chips as a source for broadband wavelength-multiplexed polarization entangled photons, Opt. Express **24**, 15160 (2016).

[33] R.-B. Jin, P. Zhao, P. Deng, and Q. L. Wu, Spectrally Pure States at Telecommunications Wavelengths from Periodically Poled $M\mathrm{TiO}X\mathrm{O}_4$ ($M = \mathrm{K}$, Rb, Cs; $X = \mathrm{P}$, As) Crystals, Phys. Rev. Applied **6**, 064017 (2016).

[34] V. G. Dmitriev, G. G. Gurzadyan, and D. N. Nikogosyan, *Handbook of Nonlinear Optical Crystals*, 3rd ed. (Springer-Verlag, Berlin, 1999).

[35] D. E. Sands, *Introduction to Crystallography* (Dover Publications, New York, 1993).

[36] F. Laudenbach, H. Hübel, M. Hentschel, and A. Poppe, QPMoptics: A novel tool to simulate and optimise photon pair creation, Proc. SPIE Int. Soc. Opt. Eng. **9894**, 98940V (2016).

[37] SNLO nonlinear optics code available from A. V. Smith, AS-Photonics, Albuquerque, NM, http://www.as-photonics.com/snlo.

[38] P. E. Powers, *Fundamentals of Nonlinear Optics*, 1st ed. (CRC Press, Boca Raton, 2011).

[39] C. K. Hong, Z. Y. Ou, and L. Mandel, Measurement of Subpicosecond Time Intervals between Two Photons by Interference, Phys. Rev. Lett. **59**, 2044 (1987).

[40] F. Kaneda, K. Garay-Palmett, A. B. U'Ren, and P. G. Kwiat, Heralded single-photon source utilizing highly nondegenerate, spectrally factorable spontaneous parametric down-conversion, Opt. Express **24**, 10733 (2016).

[41] T. Gerrits, F. Marsili, V. B. Verma, L. K. Shalm, M. Shaw, R. P. Mirin, and S. W. Nam, Spectral correlation measurements at the Hong-Ou-Mandel interference dip, Phys. Rev. A **91**, 013830 (2015).

[42] R.-B. Jin, M. Takeoka, U. Takagi, R. Shimizu, and M. Sasaki, Highly efficient entanglement swapping and teleportation at telecom wavelength, Sci. Rep. **5**, 9333 (2015).

[43] W. P. Grice, R. S. Bennink, D. S. Goodman, and A. T. Ryan, Spatial entanglement and optimal single-mode coupling, Phys. Rev. A **83**, 023810 (2011).

[44] N. Bruno, A. Martin, T. Guerreiro, B. Sanguinetti, and R. T. Thew, Pulsed source of spectrally uncorrelated and indistinguishable photons at telecom wavelengths, Opt. Express **22**, 17246 (2014).

[45] A. Gajewski and P. Kolenderski, Spectral correlation control in down-converted photon pairs, Phys. Rev. A **94**, 013838 (2016).

[46] F. König and F. N. C. Wong, Extended phase matching of second-harmonic generation in periodically poled KTiOPO_4 with zero group-velocity mismatch, Appl. Phys. Lett. **84**, 1644 (2004).

[47] K. Fradkin, A. Arie, A. Skliar, and G. Rosenman, Tunable midinfrared source by difference frequency generation in bulk periodically poled KTiOPO_4, Appl. Phys. Lett. **74**, 914 (1999).

[48] K. Kato and E. Takaoka, Sellmeier and thermo-optic dispersion formulas for KTP, Appl. Opt. **41**, 5040 (2002).

[49] T. Mikami, T. Okamoto, and K. Kato, Sellmeier and thermo-optic dispersion formulas for $\mathrm{RbTiOPO}_4$, Opt. Mater. (Amsterdam, Neth.) **31**, 1628 (2009).

[50] K. Kato, Second-harmonic and sum-frequency generation in $KTiOAsO_4$, IEEE J. Quantum Electron. **30**, 881 (1994).
[51] L. T. Cheng, L. K. Cheng, J. D. Bierlein, and F. C. Zumsteg, Nonlinear optical and electro-optical properties of single crystal $CsTiOAsO_4$, Appl. Phys. Lett. **63**, 2618 (1993).
[52] L. K. Cheng, L. T. Cheng, J. Galperin, P. A. M. Hotsenpiller, and J. D. Bierlein, Crystal growth and characterization of $KTiOPO_4$ isomorphs from the self-fluxes, J. Cryst. Growth **137**, 107 (1994).
[53] R. H. Hadfield and G. Johansson, *Superconducting Devices in Quantum Optics* (Springer-Verlag, Berlin, 2016).
[54] F. Marsili, V. Verma, M. J. Stevens, J. A. Stern, M. D. Shaw, A. Miller, D. Schwarzer, A. Wodtke, R. P. Mirin, and S. W. Nam, Quasi-phase-matched waveguide devices for generation of postselection-free polarization-entangled twin photons, in *Proceedings of CLEO: Science and Innovations, San Jose, 2013* (Optical Society of America, Washington, DC, 2013), p. CTu1H-1.
[55] T. Suhara, G. Nakaya, J. Kawashima, and M. Fujimura, Quasi-phase-matched waveguide devices for generation of postselection-free polarization-entangled twin photons, IEEE Photonics Technol. Lett. **21**, 1096 (2009).
[56] H. Herrmann, X. Yang, A. Thomas, A. Poppe, W. Sohler, and C. Silberhorn, Post-selection free, integrated optical source of non-degenerate, polarization entangled photon pairs, Opt. Express **21**, 27981 (2013).